

# Thermal conductivity of Magnesium Telluride (MgTe) - A first principles study

Rajmohan Muthaiah, Jivtesh Garg

School of Aerospace and Mechanical Engineering, University of Oklahoma, Norman,

OK-73019, USA

**Abstract:** In this work, we report thermal conductivity( $k$ ) of magnesium telluride (MgTe) with various crystallographic phases such as rocksalt, zincblende, wurtzite and nickel arsenic (NiAs) using density functional theory and Boltzmann transport equation. Our first principles calculations results show the low thermal conductivity of MgTe with  $k_{\text{NiAs}} < k_{\text{rocksalt}} < k_{\text{wurtzite}} < k_{\text{zincblende}}$ . We systematically investigated the phonon group velocity, phonon scattering rate and mode contributed thermal conductivity of transverse acoustic (TA), longitudinal acoustic (LA) and optical phonons. Our first principles calculations shows that ultra-low thermal conductivity of  $2.645 \text{ Wm}^{-1}\text{K}^{-1}$  for NiAs phase is due to the dominant scattering of TA and LA phonons by low frequency optical phonons. We also analyzed the length dependence thermal conductivity of MgTe at nanometer length-scales. At nanometer length scales such as 50 nm for NiAs phase, room temperature thermal conductivity of less than  $1.4 \text{ Wm}^{-1}\text{K}^{-1}$  shows a promising nature of MgTe for thermoelectric applications.

**Keywords:** Magnesium, Telluride, MgTe, Semiconductors, thermal conductivity, thermoelectric, first principles calculations.

**Introduction:** Magnesium chalcogenides-based semiconductors have attracted both scientific and technological applications<sup>1-3</sup>. Magnesium<sup>4-7</sup> and Telluride<sup>8-14</sup> based thermoelectric and photovoltaic materials are getting attention among the scientific community due to its ultra-low thermal conductivity and tunable electronic bandgap. Magnesium telluride(MgTe) is extensively studied for its structural<sup>1, 2, 15, 16</sup>, electronic<sup>1-3, 15</sup>, elastic<sup>15</sup>, magnetic<sup>1, 2</sup>, optical<sup>15</sup> and vibrational<sup>3, 17</sup> properties. Despite these extensive studies, thermal conductivities of MgTe are unknown and inspiring us to compute it for all the crystalline phases. Thermal conductivity of a material is critical for wide varieties of application such as thermal management system<sup>18-25</sup>, thermoelectrics<sup>26-28</sup>, opto-electronics<sup>29</sup> and solar cells<sup>30, 31</sup> etc., MgTe are known to exist in four crystalline phases such as zinc-blende (ZB), rocksalt (RS), wurtzite (WZ)<sup>3, 32, 33</sup> and nickel arsenic

(NiAs). In this work, we report bulk and nanoscale thermal conductivity of all the four crystalline phases of MgTe using density functional theory and phonon Boltzmann transport equation. We also report an ultra-low thermal conductivity of MgTe at nanometer length scales. We systematically investigated the elastic constants, phonon group velocity, phonon bandgap and phonon scattering rate (inverse of phonon lifetime) for all the crystalline phases. At 300 K, bulk thermal conductivity of 2.645(NiAs), 6.26(RS), 8.83(WZ) and 10.05(ZB)  $\text{Wm}^{-1}\text{K}^{-1}$  shows that MgTe will be a promising thermoelectric material. These results have important implications for applications of MgTe in thermoelectric energy conversion techniques, solar-cells and other optoelectronics.

### Computational Methods:

All the first principles calculations were performed using QUANTUM ESPRESSO<sup>34</sup> package. Norm-conserving pseudopotential with local density approximation (LDA)<sup>35</sup> exchange-correlation functional is used to approximate the MgTe. The geometry of the zinc-blende and rocksalt MgTe with 2 atoms (4 atoms for wurtzite and NiAs) unit cell were optimized until forces on all atoms were less than  $10^{-6}$  Ry/bohr. Plane-wave energy cutoff of 80 Ry and  $8 \times 8 \times 8$  ( $12 \times 12 \times 8$ ) Monkhorst-Pack<sup>36</sup>  $k$ -point mesh were used integrate over the Brillouin zone. Relaxed structure with equilibrium lattice constants of MgTe with different lattice crystal phases are shown in Fig 1

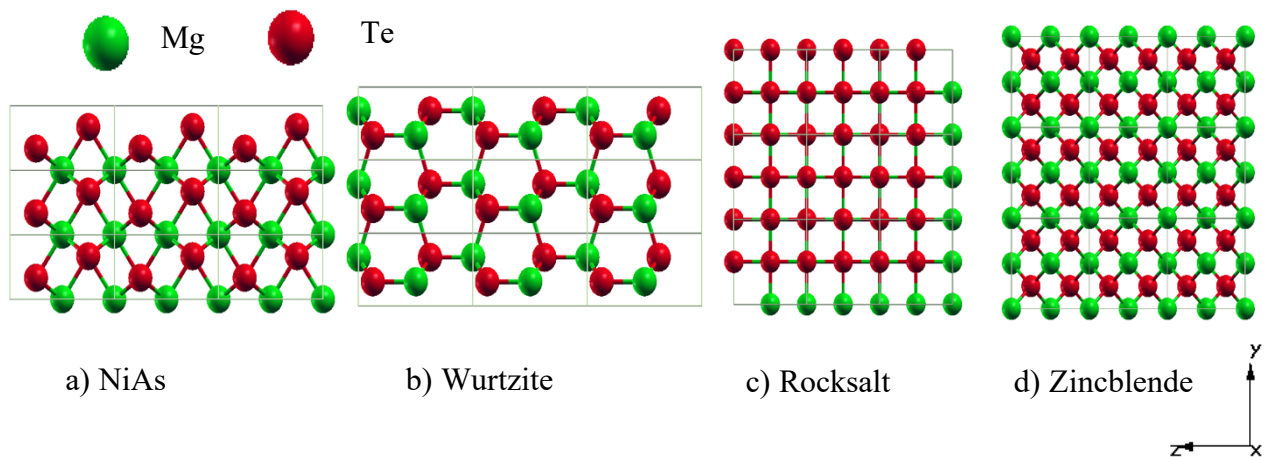


Figure 1a-d): Crystal structure of MgTe with crystalline phases; NiAs ( $a=7.8585$  bohr,  $c/a=1.6281$ ), wurtzite ( $a=8.5287$  bohr,  $c/a=1.6286$ ), rocksalt ( $a=11.0985$  bohr) and zinblende ( $a=12.073$  bohr) respectively.

and also listed in Table 1 which are in excellent agreement with previously published values G.P.Srivatsava *et.al*<sup>3</sup>.

Lattice thermal conductivity( $k$ ) was computed by solving phonon Boltzmann transport equation (PBTE)<sup>37</sup> in both single mode relaxation approximation (SMRT) and iteratively using a variational method. Expression for thermal conductivity ( $k$ ) obtained by solving PBTE in the single mode relaxation time (SMRT) approximation<sup>38</sup> is given by,

$$k_{\alpha} = \frac{\hbar^2}{N\Omega k_b T^2} \sum_{\lambda} v_{\alpha\lambda}^2 \omega_{\lambda}^2 \bar{n}_{\lambda} (\bar{n}_{\lambda} + 1) \tau_{\lambda} \quad (1)$$

where,  $\alpha$ ,  $\hbar$ ,  $N$ ,  $\Omega$ ,  $k_b$ ,  $T$ , are the cartesian direction, Planck constant, size of the  $\mathbf{q}$  mesh, unit cell volume, Boltzmann constant, and absolute temperature respectively.  $\lambda$  represents the vibrational mode ( $\mathbf{q}^j$ ) ( $\mathbf{q}$  is the wave vector and  $j$  represent phonon polarization).  $\omega_{\lambda}$ ,  $\bar{n}_{\lambda}$ , and  $v_{\alpha\lambda}$  ( $= \partial\omega_{\lambda}/\partial q$ ) are the phonon frequency, equilibrium Bose-Einstein population and group velocity along cartesian direction  $\alpha$ , respectively of a phonon mode  $\lambda$ .  $\omega_{\lambda}$ ,  $\bar{n}_{\lambda}$ , and  $c_{\alpha\lambda}$  are derived from the knowledge of phonon dispersion computed using 2<sup>nd</sup> order IFCs.  $\tau_{\lambda}$  is the phonon lifetime and is computed using the equation,

$$\frac{1}{\tau_{\lambda}} = \pi \sum_{\lambda'\lambda''} |V_3(-\lambda, \lambda', \lambda'')|^2 \times [2(n_{\lambda'} - n_{\lambda''})\delta(\omega(\lambda) + \omega(\lambda') - \omega(\lambda'')) + (1 + n_{\lambda'} + n_{\lambda''})\delta(\omega(\lambda) - \omega(\lambda') - \omega(\lambda''))] \quad (2)$$

where,  $\frac{1}{\tau_{\lambda}}$  is the anharmonic scattering rate based on the lowest order three phonon interactions and  $V_3(-\lambda, \lambda', \lambda'')$  are the three-phonon coupling matrix elements computed using both harmonic (2<sup>nd</sup> derivative of energy) and anharmonic (3<sup>rd</sup> derivative of energy) interatomic force constants. 2<sup>nd</sup> and 3<sup>rd</sup> order interatomic force constants were derived from density-functional perturbation theory (DFPT)<sup>39, 40</sup>. Harmonic force constants for ZB and RS systems were calculated on 8 x 8 x 8(9 x 9 x 6 for WZ and NiAs) q-grid. Anharmonic force constants for ZB and RS were computed on a 4 x 4 x 4 (3 x 3 x 2 for WZ and NiAs) q point grid using D3Q<sup>37, 41, 42</sup> package within QUANTUM-ESPRESSO. Acoustic sum rules were imposed on both harmonic and anharmonic interatomic force constants. Phonon linewidth and lattice thermal conductivity were calculated using ‘thermal2’ package within QUANTUM ESPRESSO. For these calculations, 30 x 30 x 30(for ZB and RS) and 30 x 30 x 20(for WZ and NiAs) q -mesh was used and iterations in the exact solution of the PBTE were performed until  $\Delta k$  between consecutive iterations diminished to below  $1.0e^{-5}$ .  $k$  values were converged after 5 iterations. Casimir scattering<sup>43</sup> is imposed to include the effect of boundary scattering for computing length dependent thermal conductivity in the nanoscales.

Elastic constants were computed using ‘thermo\_pw’ package in QUANTUM-ESPRESSO; Voigt-Reuss-Hill approximation<sup>44</sup> was used to calculate Bulk modulus, Shear modulus(G), Young’s Modulus(E) and Poisson’s ratio( $\nu$ ).

**Results and Discussion:** Phonon dispersion and phonon density of states for the four crystalline phases of MgTe is shown in Fig 1 which are in good agreement with previous work<sup>3</sup>. Structural parameters such as Young’s modulus(E), Bulk modulus(B), Shear modulus(G) and Poisson’s ratio computed based on Voigt-Reuss-Hill approximation are listed in Table 1 which are also in excellent agreement with the previously published work<sup>3, 17</sup> for all the four crystalline phases of MgTe.

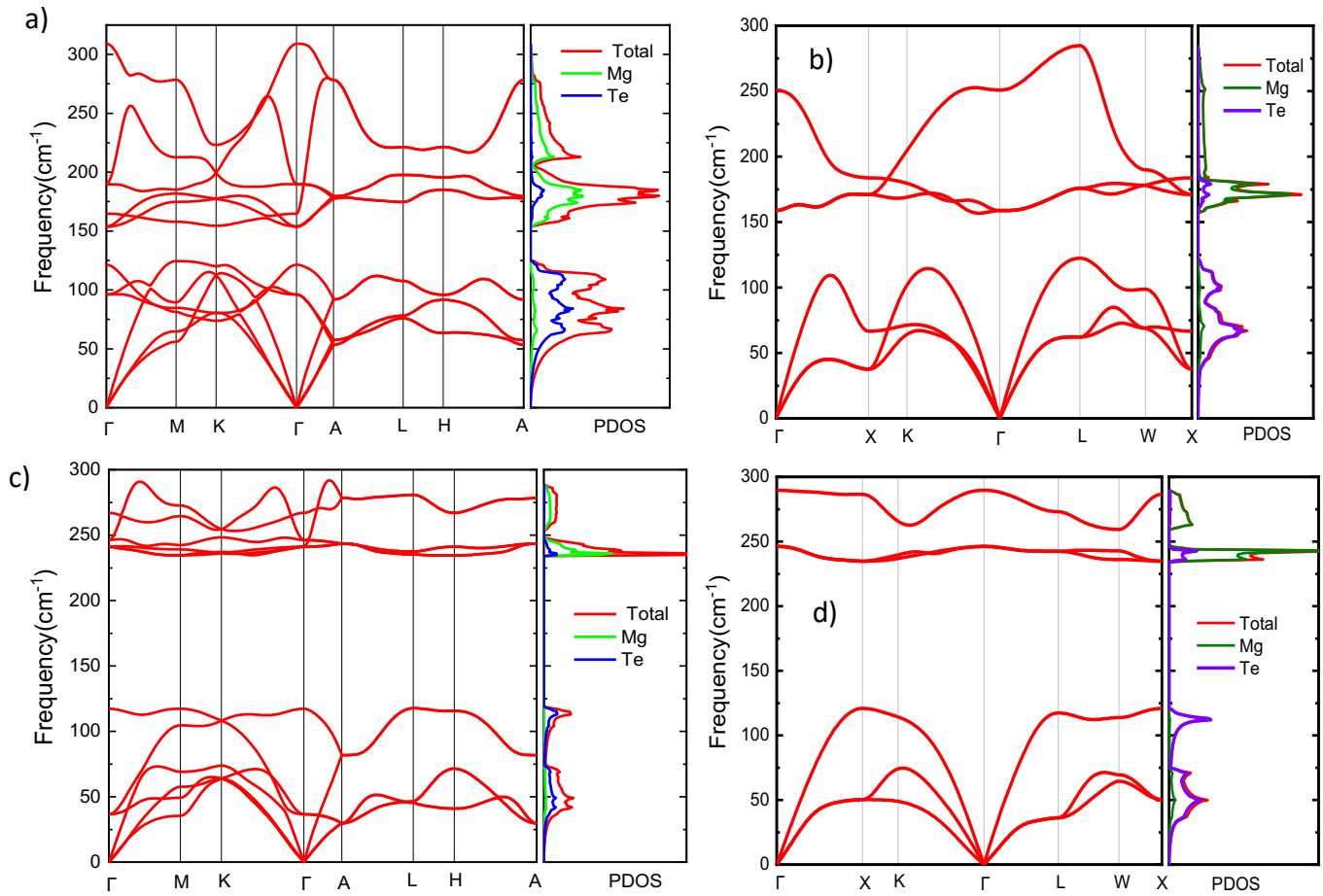


Figure 2: Phonon dispersion and phonon density of states for the MgTe with crystal phase a) nickel arsenic b) rocksalt c) wurtzite and d) zincblende



**Table 1: Lattice constants, Bulk modulus(B), Youngs modulus(E), Shear modulus(G) and poisson's( $\nu$ ) ratio of MgTe with different crystal phase.**

S. No	Crystal phase	a (bohr)	c/a	B (GPa)	E(GPa)	G(GPa)	$\nu$
1.	Nickel arsenic (NiAs)	7.8585	1.6281	52.82	63.97	24.64	0.2981
2.	Wurtzite (WZ)	8.5287	1.6286	38.97	44.92	17.18	0.3076
3.	Rocksalt (RS)	11.0985		52.7	86.12	35.07	0.2276
4.	Zincblende (ZB)	12.073		38.39	37.1	13.88	0.3367

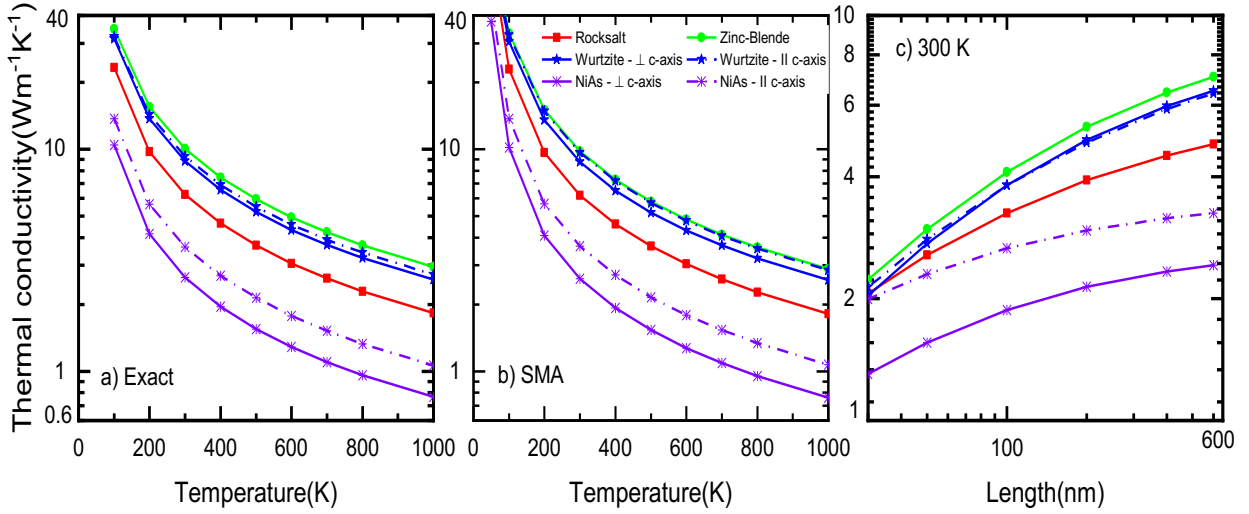


Figure 3a Temperature dependent lattice thermal conductivity by solving the PBTE iteratively b) at single mode relaxation time approximation (SMA) c) Length dependence thermal conductivity at room temperature (300 K) for MgTe with different crystalline phase.

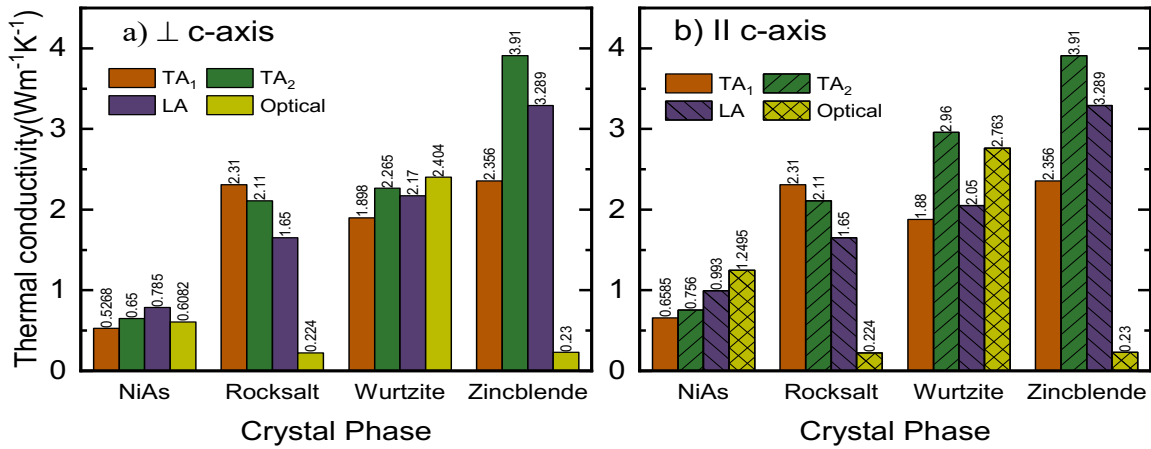


Figure 4: Thermal conductivity contribution from TA<sub>1</sub>, TA<sub>2</sub>, LA and optical phonon modes of MgTe with different crystalline phase along different directions.

Lattice thermal conductivity( $k$ ) calculated by solving the phonon Boltzmann transport equation (PBTE) is shown in Fig 3. Fig 3a and b represents the temperature dependent lattice thermal conductivity of MgTe with different crystalline phase by solving the PBTE iteratively and at SMA. SMA results are just 5% less than that of the iterative solutions. At 300 K, full

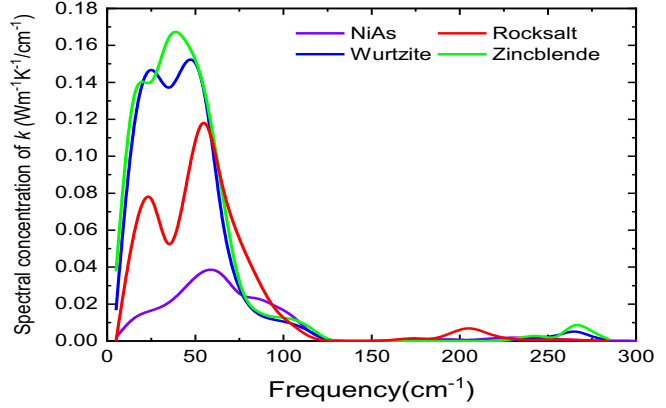


Figure 5: Spectral distributions of thermal conductivity in MgTe with different crystalline phase.

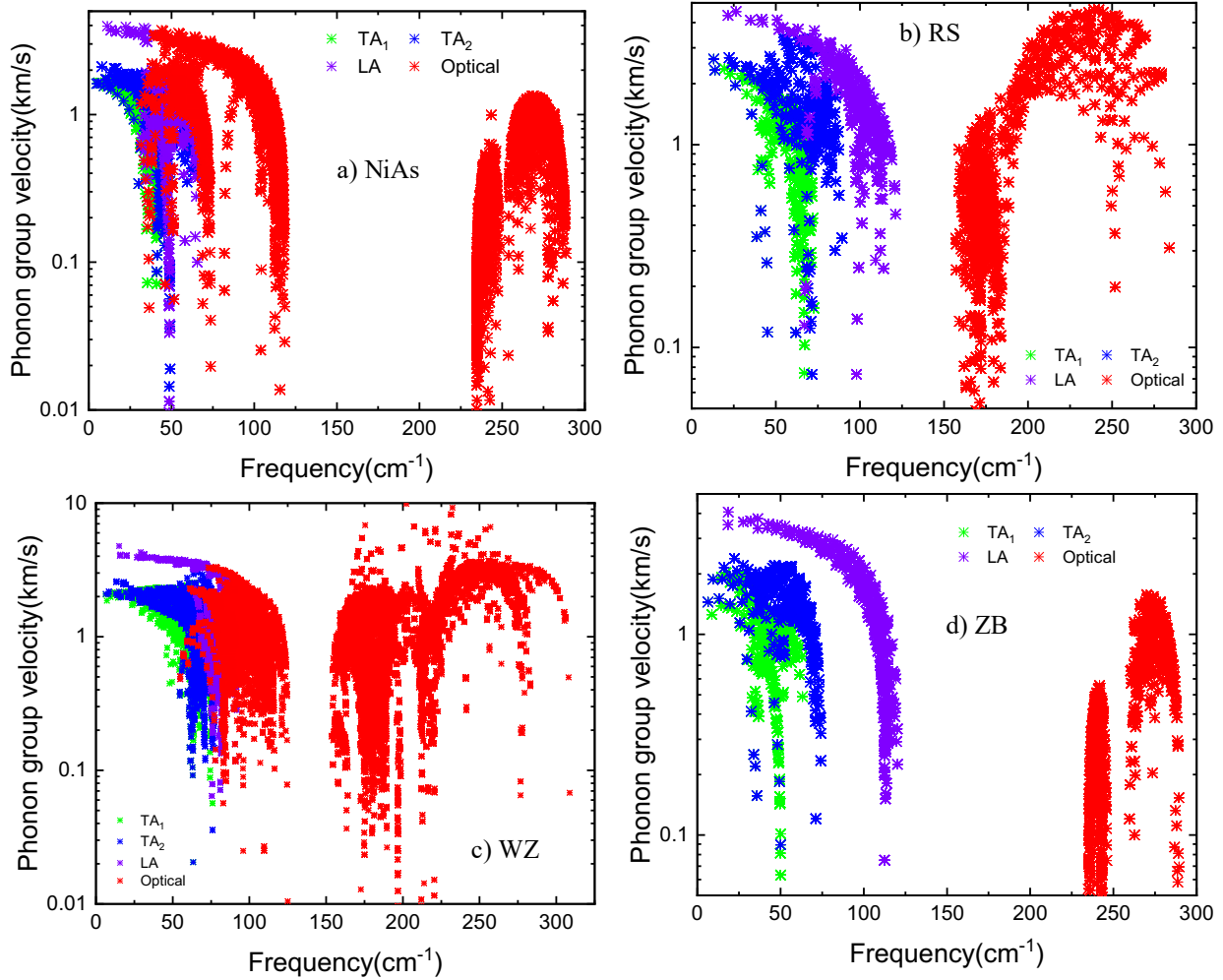


Figure 7 : Phonon group velocity of MgTe with crystalline phase a) nickel arsenic (NiAs) b) rocksalt (RS) b) wurtzite (WZ) d) zinblend (ZB) at 300K

iterated thermal conductivity( $k$ ) of MgTe is as follows:  $k_{\text{NiAs}}(2.645 \text{ Wm}^{-1}\text{K}^{-1}) < k_{\text{RS}}(6.26 \text{ Wm}^{-1}\text{K}^{-1}) < k_{\text{WZ}}(8.83 \text{ Wm}^{-1}\text{K}^{-1}) < k_{\text{ZB}}(10.05 \text{ Wm}^{-1}\text{K}^{-1})$ . These low thermal conductivity of less than  $\sim 10 \text{ Wm}^{-1}\text{K}^{-1}$  shows the promising nature of MgTe in thermoelectric applications.  $k$  of  $10.05 \text{ Wm}^{-1}\text{K}^{-1}$  for the zincblende phase MgTe is 3.8 times of the  $k$  of NiAs phase. This is due to the large phonon bandgap ( $\sim 100 \text{ cm}^{-1}$ ) which eliminates the phonon scattering rates. Whereas ultra-low thermal conductivity of  $2.645 \text{ Wm}^{-1}\text{K}^{-1}$  for the NiAs phase is due to the acoustic phonons are scattered by low frequency optical phonons because of the less phonon bandgap ( $\sim 25 \text{ cm}^{-1}$ ). To explain this, we have analyzed the mode contributions thermal conductivity of transverse acoustic (TA<sub>1</sub>, TA<sub>2</sub>), longitudinal acoustic (LA) and optical phonon modes, phonon group velocities, phonon linewidths (scattering rates) and its spectral distribution.

Figure 4 represents the thermal conductivity contribution from each phonon mode along  $\perp$  and  $\parallel$  to the c-axis (For cubic MgTe  $k$  along  $\perp$  - c-axis and  $\parallel$  - c-axis are same) at single-mode relaxation time approximation. For the cubic systems, optical phonon contributions are less than  $\sim 3.5 \%$ . Whereas optical phonons has a major contributions in both wurtzite and Nias crystal phase due to the low frequency optical phonons. For an example,  $1.245 \text{ Wm}^{-1}\text{K}^{-1}$  along the c-axis for with NiAs phase is 34.2% to its overall thermal conductivity and is higher than both TA and LA phonon modes. Likewise,  $2.404 \text{ Wm}^{-1}\text{K}^{-1}$  along  $\perp$  -c-axis is 27.5 % to its overall thermal conductivity in wurtzite MgTe. To understand this, we plotted a spectral distribution of thermal conductivity over the entire frequency (Fig. 5) and we can observe that, low frequency optical phonons has significant contributions to its overall thermal thermal conductivity. Whereas in cubic (NiAs and ZB) MgTe, TA modes between  $25 - 75 \text{ cm}^{-1}$  has a major contribution to its overall thermal conductivity. To illustrate this further, we have plotted the phonon group velocities and phonon linewidths for all the crystalline phases in Fig. 6 and Fig. 7.

Fig 6 a-d represents the phonon group velocities of MgTe with different crystalline phase. We can observe that, low frequency optical phonons (less than  $130 \text{ cm}^{-1}$ ) has a considerable phonon group velocities to that of the acoustic phonons in NiAs and wurtzite phase. Fig 7 a-d shows the phonon linewidth for MgTe with different crystalline phase. In cubic systems, zincblende has the lowest phonon linewidth (less than  $2 \text{ cm}^{-1}$ ) for acoustic modes due to large phonon bandgap and has the highest thermal conductivity ( $\sim 10 \text{ Wm}^{-1}\text{K}^{-1}$ ) whereas TA phonons in rocksalt has one order of

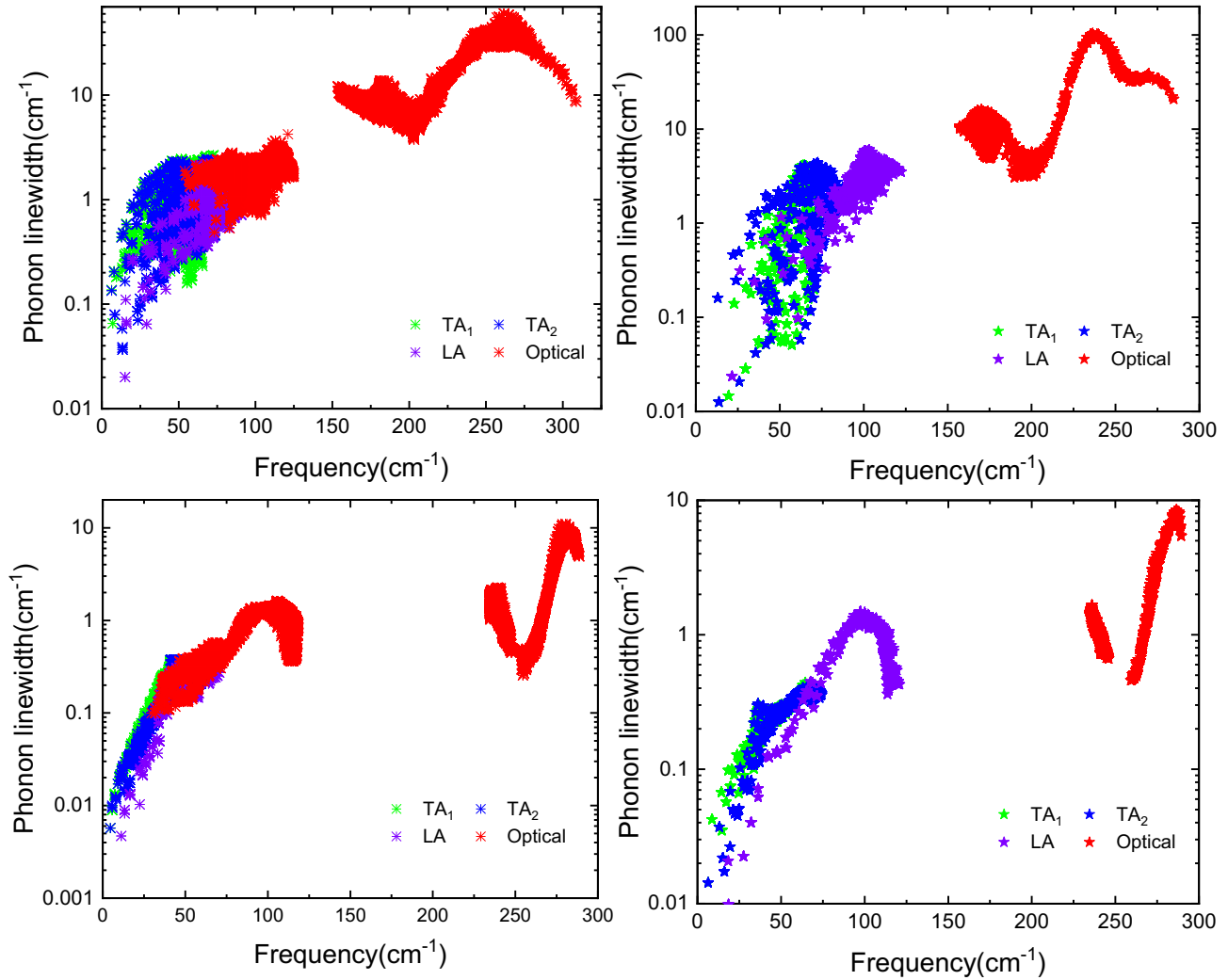


Figure 4 : Phonon linewidths of MgTe for the crystalline phase a) nickel arsenic (NiAs) b) rocksalt (RS) c) wurtzite (WZ) and zincblende (ZB) at 300K.

magnitude higher scattering rate than of the zincblende and has low thermal conductivity. Likewise, TA and LA phonons in NiAs has 8 times scattering rate than its counterpart wurtzite structure. Optical phonons in NiAs has considerable phonon lifetime (inverse of scattering rate) and hence has a significant contribution to its overall thermal conductivity.

For the nanostructures, length dependent thermal conductivity of MgTe between 30 nm and 1000 nm is computed by introducing the boundary/Casimir scattering and is shown in Fig 3c. At 300K and at 100 nm, zincblende has a maximum thermal conductivity of  $\sim 4 \text{ Wm}^{-1}\text{K}^{-1}$  shows the promising nature of MgTe for the thermoelectric applications.

**Conclusion:** In this work, thermal conductivity of magnesium telluride (MgTe) with four crystalline phases; zincblende, rocksalt, wurtzite and nickel arsenic were computed by first principles calculations with phonon Boltzmann transport equations. Our first principles calculations shows a low thermal conductivity of less than  $\sim 10 \text{ Wm}^{-1}\text{K}^{-1}$  for all the crystalline phase of MgTe. We systematically investigated the phonon group velocity, phonon scattering rate and mode dependent thermal conductivity of MgTe. Our first principles calculations shows that, NiAs and wurtzite has significant contributions from optical phonons than ZB and rocksalt. At nanometer length scales such as 50 nm for NiAs phase, thermal conductivity of less than  $1.4 \text{ Wm}^{-1}\text{K}^{-1}$  shows a promising nature of MgTe for thermoelectric applications.

**Acknowledgements:** R.M and J.G would like to acknowledge OU Supercomputing Center for Education Research (OSKER) for providing computational resources. J.G and R.M acknowledge financial support from NSF CAREER grant, Award # 1847129.

## References:

1. Akinlami, J. O., Electronic, structural and paramagnetic properties of magnesium telluride. *Semiconductors* a) NiAs *quantum electronics and optoelectronics* b) RS *5-10*.
2. Sajid, M.; H. X.; Noor, N. A.; Alay-e-Abbas, M.; Abid, M.; Shaukat, A., Theoretical Investigation of Structural, Electronic, and Magnetic Properties of V-Doped MgSe and MgTe Semiconductors. *Journal of Superconductivity and Novel Magnetism* **2014**, *27* (10), 2327-2336.
3. Duman, S.; Bağcı, S.; Tütüncü, H. M.; Srivastava, G. P., First-principles studies of ground-state and dynamical properties of MgS, MgSe, and MgTe in the rocksalt, zinc blende, wurtzite, and nickel arsenide phases. *Physical Review B* **2006**, *73* (20), 205201.
4. Condrón, C. L.; Kauzlarich, S. M.; Gascoin, F.; Snyder, G. J., Thermoelectric properties and microstructure of Mg<sub>3</sub>Sb<sub>2</sub>. *Journal of Solid State Chemistry* **2006**, *179* (8), 2252-2257.
5. Zhang, J.; Song, L.; Pedersen, S. H.; Yin, H.; Hung, L. T.; Iversen, B. B., Discovery of high-performance low-cost n-type Mg<sub>3</sub>Sb<sub>2</sub>-based thermoelectric materials with multi-valley conduction bands. *Nature Communications* **2017**, *8* (1), 13901.
6. Li, H.; Zhang, S.; Fang, T.; Yue, L.; Zhang, S.; Lu, G., First-principles prediction of a high ZT of n-type *c*) WZ *compounds with isotropic thermal conductivity* d) ZB *duction performance*. *Physical Chemistry Chemical Physics* **2018**, *20* (11), 7686-7693.
7. Zhang, F.; Chen, C.; Yao, H.; Bai, F.; Yin, L.; Li, X.; Li, S.; Xue, W.; Wang, Y.; Cao, F.; Liu, X.; Sui, J.; Zhang, Q., High-Performance N-type Mg<sub>3</sub>Sb<sub>2</sub> towards Thermoelectric Application near Room Temperature. *Advanced Functional Materials* **2020**, *30* (5), 1906143.
8. Khusainov, A. K., Cadmium telluride detectors with thermoelectric cooling. *Nuclear Instruments and Methods in Physics Research Section A: Accelerators, Spectrometers, Detectors and Associated Equipment* **1992**, *322* (3), 335-340.

9. Dughaish, Z. H., Lead telluride as a thermoelectric material for thermoelectric power generation. *Physica B: Condensed Matter* **2002**, 322 (1), 205-223.
10. Hossain, M. S.; Islam, R.; Shahjahan, M.; Khan, K. A., Studies on the thermoelectric effect in semiconducting ZnTe thin films. *Journal of Materials Science: Materials in Electronics* **2008**, 19 (11), 1114-1121.
11. Zweibel, K., The Impact of Tellurium Supply on Cadmium Telluride Photovoltaics. *Science* **2010**, 328 (5979), 699-701.
12. Başol, B.; McCandless, B., Brief review of cadmium telluride-based photovoltaic technologies. *Journal of Photonics for Energy* **2014**, 4 (1), 040996.
13. Bhaskar, A.; Pai, Y.-H.; Wu, W.-M.; Chang, C.-L.; Liu, C.-J., Low thermal conductivity and enhanced thermoelectric performance of nanostructured Al-doped ZnTe. *Ceramics International* **2016**, 42 (1, Part B), 1070-1076.
14. Dmitriev, A. V., High doping effect on the thermoelectric properties of p-type lead telluride. *Journal of Applied Physics* **2018**, 123 (16), 165707.
15. Drief, F.; Tadjer, A.; Mesri, D.; Aourag, H., First principles study of structural, electronic, elastic and optical properties of MgS, MgSe and MgTe. *Catalysis Today* **2004**, 89 (3), 343-355.
16. Kuhn, A.; Chevy, A.; Naud, M.-J., Preparation and some physical properties of magnesium telluride single crystals. *Journal of Crystal Growth* **1971**, 9, 263-265.
17. Gökoğlu, G., First principles vibrational dynamics of magnesium telluride. *Journal of Physics and Chemistry of Solids* **2010**, 71 (9), 1388-1392.
18. Chen, G.; Shakouri, A., Heat Transfer in Nanostructures for Solid-State Energy Conversion. *Journal of Heat Transfer* **2001**, 124 (2), 242-252.
19. Bar-Cohen, A.; Wang, P.; Rahim, E., Thermal management of high heat flux nanoelectronic chips. *Microgravity Science and Technology* **2007**, 19 (3), 48-52.
20. Anandan, S. S.; Ramalingam, V. In *Thermal management of electronics: A review of literature*, 2008.
21. Lindsay, L.; Broido, D. A.; Reinecke, T. L., First-Principles Determination of Ultrahigh Thermal Conductivity of Boron Arsenide: A Competitor for Diamond? *Physical Review Letters* **2013**, 111 (2), 025901.
22. Muthaiah, R.; Garg, J., Temperature effects in the thermal conductivity of aligned amorphous polyethylene—A molecular dynamics study. *Journal of Applied Physics* **2018**, 124 (10), 105102.
23. Muthaiah, R.; Garg, J., Strain tuned high thermal conductivity in boron phosphide at nanometer length scales – a first-principles study. *Physical Chemistry Chemical Physics* **2020**, 22 (36), 20914-20921.
24. Tarannum, F.; Muthaiah, R.; Annam, R. S.; Gu, T.; Garg, J., Effect of Alignment on Enhancement of Thermal Conductivity of Polyethylene–Graphene Nanocomposites and Comparison with Effective Medium Theory. *Nanomaterials* **2020**, 10 (7), 1291.
25. Muthaiah, R.; Tarannum, F.; Annam, R. S.; Nayal, A. S.; Danayat, S.; Garg, J., Thermal conductivity of hexagonal BC2P – a first-principles study. *RSC Advances* **2020**, 10 (70), 42628-42632.
26. Yang, B.; Li, S.; Li, X.; Liu, Z.; Zhong, H.; Feng, S., Ultralow thermal conductivity and enhanced thermoelectric properties of SnTe based alloys prepared by melt spinning technique. *Journal of Alloys and Compounds* **2020**, 837, 155568.

27. Malhotra, A.; Maldovan, M., Phononic pathways towards rational design of nanowire heat conduction. *Nanotechnology* **2019**, *30* (37), 372002.
28. Hori, T.; Shiomi, J., Tuning phonon transport spectrum for better thermoelectric materials. *Sci Technol Adv Mater* **2019**, *20* (1), 10-25.
29. Oh, S. K.; Lundh, J. S.; Shervin, S.; Chatterjee, B.; Lee, D. K.; Choi, S.; Kwak, J. S.; Ryou, J.-H., Thermal Management and Characterization of High-Power Wide-Bandgap Semiconductor Electronic and Photonic Devices in Automotive Applications. *Journal of Electronic Packaging* **2019**, *141* (2).
30. Chauhan, A.; Tyagi, V. V.; Anand, S., Futuristic approach for thermal management in solar PV/thermal systems with possible applications. *Energy Conversion and Management* **2018**, *163*, 314-354.
31. Saadah, M. In *Thermal Management of Solar Cells*, 2013.
32. Yanagisawa, S.; Tashiro, M.; Anzai, S., Crystal structure of magnesium ditelluride. *Journal of Inorganic and Nuclear Chemistry* **1969**, *31* (4), 943-946.
33. Klemm, W.; Wahl, K., Notiz Über das Magnesiumtellurid. *Zeitschrift für anorganische und allgemeine Chemie* **1951**, *266* (6), 289-292.
34. Giannozzi, P.; Baroni, S.; Bonini, N.; Calandra, M.; Car, R.; Cavazzoni, C.; Ceresoli, D.; Chiarotti, G. L.; Cococcioni, M.; Dabo, I.; Dal Corso, A.; de Gironcoli, S.; Fabris, S.; Fratesi, G.; Gebauer, R.; Gerstmann, U.; Gougoussis, C.; Kokalj, A.; Lazzeri, M.; Martin-Samos, L.; Marzari, N.; Mauri, F.; Mazzarello, R.; Paolini, S.; Pasquarello, A.; Paulatto, L.; Sbraccia, C.; Scandolo, S.; Sclauzero, G.; Seitsonen, A. P.; Smogunov, A.; Umari, P.; Wentzcovitch, R. M., QUANTUM ESPRESSO: a modular and open-source software project for quantum simulations of materials. *Journal of Physics: Condensed Matter* **2009**, *21* (39), 395502.
35. Ceperley, D. M.; Alder, B. J., Ground State of the Electron Gas by a Stochastic Method. *Physical Review Letters* **1980**, *45* (7), 566-569.
36. Monkhorst, H. J.; Pack, J. D., Special points for Brillouin-zone integrations. *Physical Review B* **1976**, *13* (12), 5188-5192.
37. Fugallo, G.; Lazzeri, M.; Paulatto, L.; Mauri, F., Ab initio variational approach for evaluating lattice thermal conductivity. *Physical Review B* **2013**, *88* (4), 045430.
38. Srivastava, G. P., *The Physics of Phonons*. Taylor & Francis: 1990.
39. Debernardi, A.; Baroni, S.; Molinari, E., Anharmonic Phonon Lifetimes in Semiconductors from Density-Functional Perturbation Theory. *Physical Review Letters* **1995**, *75* (9), 1819-1822.
40. Deinzer, G.; Birner, G.; Strauch, D., Ab initio calculation of the linewidth of various phonon modes in germanium and silicon. *Physical Review B* **2003**, *67* (14), 144304.
41. Paulatto, L.; Errea, I.; Calandra, M.; Mauri, F., First-principles calculations of phonon frequencies, lifetimes, and spectral functions from weak to strong anharmonicity: The example of palladium hydrides. *Physical Review B* **2015**, *91* (5), 054304.
42. Paulatto, L.; Mauri, F.; Lazzeri, M., Anharmonic properties from a generalized third-order ab initio approach: Theory and applications to graphite and graphene. *Physical Review B* **2013**, *87* (21), 214303.
43. Casimir, H. B. G., Note on the conduction of heat in crystals. *Physica* **1938**, *5* (6), 495-500.
44. Chung, D. H.; Buessem, W. R., The Voigt-Reuss-Hill (VRH) Approximation and the Elastic Moduli of Polycrystalline ZnO, TiO<sub>2</sub> (Rutile), and  $\alpha$ -Al<sub>2</sub>O<sub>3</sub>. *Journal of Applied Physics* **1968**, *39* (6), 2777-2782.

